Nanomaterials for Cancer Therapy

Deutsche Ausgabe: DOI: 10.1002/ange.201605509
Internationale Ausgabe: DOI: 10.1002/anie.201605509

Copper(II)–Graphitic Carbon Nitride Triggered Synergy: Improved ROS Generation and Reduced Glutathione Levels for Enhanced Photodynamic Therapy

Enguo Ju, Kai Dong, Zhaowei Chen, Zhen Liu, Chaoqun Liu, Yanyan Huang, Zhenzhen Wang, Fang Pu, Jinsong Ren, and Xiaogang Qu**

Abstract: *Graphitic carbon nitride (g-C_3N_4) has been used as photosensitizer to generate reactive oxygen species (ROS) for photodynamic therapy (PDT). However, its therapeutic efficiency was far from satisfactory. One of the major obstacles was the overexpression of glutathione (GSH) in cancer cells, which could diminish the amount of generated ROS before their arrival at the target site. Herein, we report that the integration of Cu^{2+} and g-C_3N_4 nanosheets (Cu^{2+}–g-C_3N_4) led to enhanced light-triggered ROS generation as well as the depletion of intracellular GSH levels. Consequently, the ROS generated under light irradiation could be consumed less by reduced GSH, and efficiency was improved. Importantly, redox-active species Cu^{+}–g-C_3N_4 could catalyze the reduction of molecular oxygen to the superoxide anion or hydrogen peroxide to the hydroxyl radical, both of which facilitated the generation of ROS. This synergy of improved ROS generation and GSH depletion could enhance the efficiency of PDT for cancer therapy.*

Ultrathin two-dimensional (2D) nanomaterials have sparked increasing interest owing to their unique structural and electronic properties over the past decade.[1] Tremendous effort has been devoted to the development of synthetic methods as well as potential applications in electronics/optoelectronics,[2] catalysis,[3] energy storage,[4] and biosensors.[5] In particular, 2D graphitic carbon nitride (g-C_3N_4) has shown extraordinary catalytic activity and selectivity owing to its appropriate band gap, Lewis basic functionalities, and high specific surface area.[6] Most notably, the electronic structure of g-C_3N_4, with graphitic planes formed by triazine units, could provide a visible light response, which demonstrated the potential of g-C_3N_4 as a photosensitizer for the generation of reactive oxygen species (ROS) for photodynamic therapy (PDT).[7] However, its therapeutic efficiency was far from satisfactory. One of the major obstacles was the overexpression of glutathione (GSH), which could diminish the amount of generated ROS before their arrival at the target site and greatly reduce the efficiency of therapy.[8] Little progress has been made in this regard, mainly owing to the lack of stable and efficient systems assembled with g-C_3N_4 to deplete GSH levels.[9] Therefore, the construction of a g-C_3N_4-based system with the ability to reduce intracellular GSH levels is required to improve the efficiency of photodynamic therapy.

Recently, considerable attention has been directed towards the employment of metal ions in medicine because of their positive charges and stereoelectronic properties, which enable them to alter the structure and function of important biological targets. In particular, the bioactivity of copper has stimulated an extensive search owing to its redox activity, its requirement as a cofactor, and its predilection to displace other essential metals.[10] An increasing amount of evidence has suggested that the co-occurrence of copper and GSH could promote a pro-oxidant effect through a metal-reducing action.[11] In this case, the reduction of Cu^{2+} by GSH could give rise to the formation of a redox-active species capable of catalyzing the subsequent reduction of molecular oxygen to the superoxide anion, and the reduction of hydrogen peroxide to the hydroxyl radical. A recent study also demonstrated that Cu^{2+} can bind to the amine moiety on phosphatidylethanolamine lipids and react with H_2O_2 to increase the concentration of ROS.[12] Furthermore, the strong spin–orbit coupling of the heavy-metal center enhanced intersystem crossing (ISC), which invariably resulted in more ROS generation.[13] Therefore, the combination of redox-active metal ions and a photosensitizer might enable the reduction of GSH levels and improvement of the efficiency of cancer therapy.

We envisioned that the coordination of Cu^{2+} with g-C_3N_4 would enhance the efficiency of photodynamic therapy through Cu^{2+}-induced GSH depletion and a pro-oxidant effect. Herein, we report that the integration of Cu^{2+} and graphitic carbon nitride nanosheets (designated as Cu^{2+}–g-C_3N_4) led to enhanced light-triggered ROS generation as well as the depletion of intracellular GSH levels (Scheme 1). Consequently, the ROS generated under light irradiation could be consumed less by the reduced GSH, and efficiency was improved. Importantly, the redox-active species Cu^{+}–g-C_3N_4 could catalyze the reduction of molecular oxygen to the superoxide anion or hydrogen peroxide to the hydroxyl radical, both of which facilitated the generation of ROS.

We first demonstrate our concept on the basis of time-dependent density functional theory (TD-DFT) calculations

[*] E. Ju, K. Dong, Z. Chen, Z. Liu, F. Pu, Prof. J. Ren, Prof. X. Qu
Laboratory of Chemical Biology and State Key Laboratory of Rare Earth Resource Utilization
Changchun Institute of Applied Chemistry, Chinese Academy of Science, Changchun, Jilin 130022 (P.R. China)
E-mail: jren@ciac.ac.cn
xqu@ciac.ac.cn
E. Ju, C. Liu, Y. Huang, Z. Wang
University of Chinese Academy of Sciences
Beijing 100039 (P.R. China)

Supporting information for this article can be found under: http://dx.doi.org/10.1002/anie.201605509.

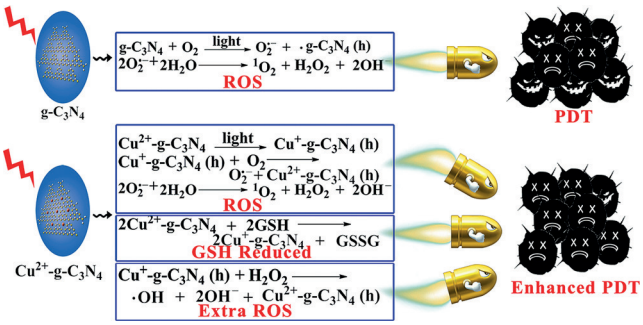

Scheme 1. Illustration of g-C_3N_4 nanosheets as photosensitizers for photodynamic therapy and Cu^{2+}–g-C_3N_4 with enhanced PDT through the synergetic effect of extra ROS generation and GSH depletion.

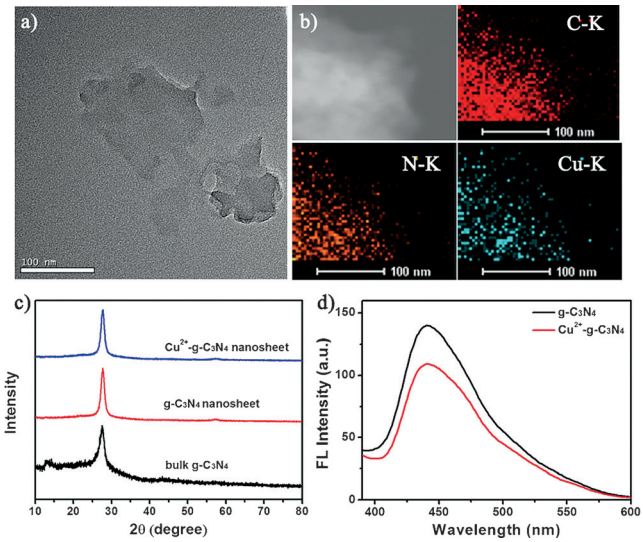

Figure 1. a) TEM image and b) dark-field TEM image of Cu^{2+}–g-C_3N_4 nanosheets and corresponding energy-dispersive spectroscopic element mapping of C K-edge, N K-edge, and Cu K-edge signals. c) XRD patterns of bulk g-C_3N_4, g-C_3N_4 nanosheets, and Cu^{2+}–g-C_3N_4 nanosheets. d) Fluorescence spectra of g-C_3N_4 and Cu^{2+}–g-C_3N_4 at the same concentration.

performed at the B3LYP/6-31g level.[14] The results indicated that Cu^{2+}–g-C_3N_4 exhibited clear separation of the HOMO and LUMO distributions as compared with g-C_3N_4 (see Figure S1 and Table S1 in the Supporting Information). This clear separation of the frontier orbitals led to a much smaller ΔE_{ST} value (energy gap between the lowest singlet excited state and the lowest triplet excited state), thus suggesting a potentially high ISC rate and thus the possibility of efficient ROS generation upon irradiation with light. To substantiate our design, we first prepared ROS-generating water-soluble g-C_3N_4 nanosheets by chemical oxidation of bulk g-C_3N_4, followed by ultrasonication-assisted liquid exfoliation. Then Cu^{2+} was ligated to g-C_3N_4 through the chelation of Cu^{2+} with N atoms in g-C_3N_4. The Lewis basic N atoms in g-C_3N_4 showed strong coordination to Cu^{2+}. Transmission electron microscopy clearly revealed that the sheet structure of Cu^{2+}–g-C_3N_4 had changed little as compared with g-C_3N_4, thus indicating that bound Cu^{2+} had no significant influence on the morphology of g-C_3N_4 (Figure 1a; see also Figure S2). Furthermore, the hydrodynamic diameter and UV/Vis absorbance of Cu^{2+}–g-C_3N_4 showed little change as compared with g-C_3N_4 (see Figures S3 and S4). The presence of Cu and g-C_3N_4 was demonstrated by element mapping by using energy-dispersive X-ray spectroscopy (Figure 1b). The actual Cu content was determined to be 0.0020 wt% by inductively coupled plasma optical emission spectroscopy (ICP-OES). By X-ray diffraction, two typical peaks at $2\theta = 13.3$ and 27.4° were observed in bulk C_3N_4. These peaks originated from interlayer structural packing and interlayer stacking of the conjugated aromatic system, respectively (Figure 1c). As for g-C_3N_4, the low-angle peak diminished, thus indicating the decreased planar size after chemical oxidation and exfoliation. No additional peak was observed after ligation, which demonstrated that Cu^{2+}–g-C_3N_4 preserved the same structure as g-C_3N_4 and no crystalline form of Cu was formed. The successful ligation of Cu^{2+} with C_3N_4 was further confirmed by the decreased fluorescence intensity, which could be explained by the ability of Cu^{2+} to capture the photoexcited electrons of g-C_3N_4, thus leading to photoluminescence quenching (Figure 1d).

The chemical structure of the as-prepared Cu^{2+}–g-C_3N_4 was further confirmed by Fourier transform infrared (FTIR) spectroscopy. The characteristic spectra of Cu^{2+}–g-C_3N_4 showed nearly identical absorption bands with g-C_3N_4 (Figure 2a), thus indicating that the coordinated Cu^{2+} did not destroy the structure of g-C_3N_4. The band at 810 cm^{-1} was attributed to the breathing of tri-*s*-triazine units, and the

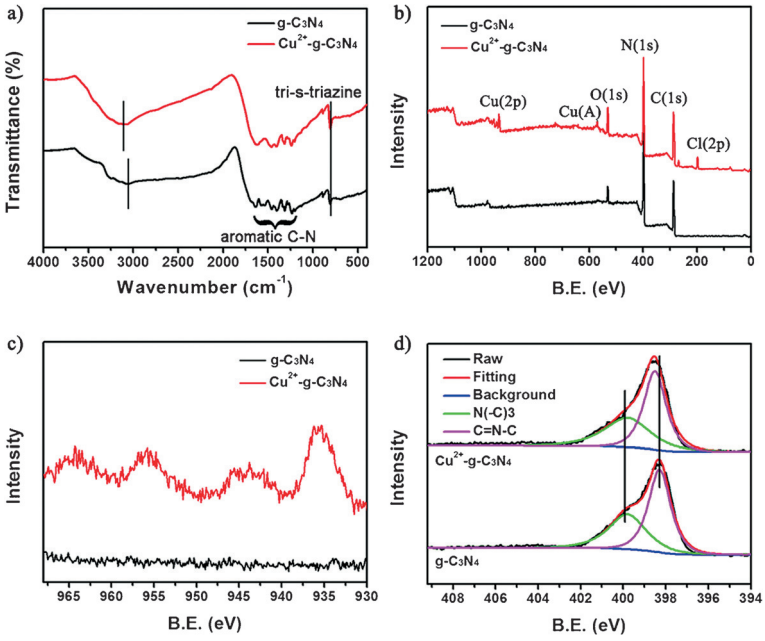

Figure 2. a) FTIR spectra and b) XPS spectra of the obtained g-C_3N_4 and Cu^{2+}–g-C_3N_4. c) Cu 2p peak and d) N 1s peak of g-C_3N_4 and Cu^{2+}–g-C_3N_4 at high resolution.

peaks in the region of 1000–1800 cm^{-1} originated from the stretching vibration of aromatic CN heterocycles. In particular, the peak at 3000–3500 cm^{-1} of Cu^{2+}–g-C_3N_4 was shifted to higher frequency, which could be attributed to the formation of Cu–N coordination bonds.[15] We further studied the chemical composition and chemical states of Cu^{2+}–g-C_3N_4 by X-ray photoelectron spectroscopy (XPS). g-C_3N_4 is mainly composed of carbon and nitrogen with small amount of oxygen adsorbed on the surface (Figure 2b). In comparison, additional Cu and Cl appeared in the Cu^{2+}–g-C_3N_4, thus indicating that Cu was coordinated with both N atoms of g-C_3N_4 and Cl atoms. The high-resolution C 1s spectrum of both Cu^{2+}–g-C_3N_4 and g-C_3N_4 could be divided into two peaks centered at 284.6 and 288.0 eV (see Figure S5). The peak located at 288.0 eV was identified as the sp^2-bonded carbon atom, whereas the other peak was the signal of standard reference carbon.

To verify the state of Cu in the Cu^{2+}–g-C_3N_4, we further analyzed the high-resolution Cu 2p spectrum. Binding-energy peaks were observed for Cu $2p_{3/2}$ and Cu $2p_{1/2}$ at 935.6 and 955.5 eV, respectively (Figure 2c), which are typical values for Cu^{2+}. Moreover, the two shakeup satellite lines observed at 943.5 and 963.9 eV are characteristic of Cu^{II} with the d^9 configuration in the ground state, thus indicating the paramagnetic chemical state of Cu^{2+}.[16] The N 1s peak of g-C_3N_4 could be deconvoluted into two discrete peaks at 398.3 and 399.8 eV (Figure 2d), which were ascribed to sp^2-hybridized N atoms (C–N=C) and tertiary N atoms ($N(C)_3$). The peak of the sp^2-bonded N atoms in Cu^{2+}–g-C_3N_4 was 0.2 eV higher than that of g-C_3N_4, whereas the peak for tertiary N atoms was unchanged. A shift in the high-binding-energy direction revealed that the electrons were transferred from N atoms in C_3N_4 to Cu ions. This result also indicated that Cu^{2+} was coordinated with the sp^2-bonded N atoms of g-C_3N_4 rather than tertiary N atoms, in accordance with the active site in g-C_3N_4. After N atoms coordinated with Cu^{2+}, their electron density decreased, thus resulting in an increase in binding energy. All results confirmed that the as-prepared Cu^{2+}–g-C_3N_4 retained the structure of g-C_3N_4, which was favorable for the following study of photoinduced ROS generation.

To test whether the ligation of Cu^{2+} could improve the PDT efficiency of C_3N_4 in the presence of GSH, we investigated ROS generation under light irradiation in a buffer. 2′,7′-Dichlorofluorescein (DCF) was employed as a probe to evaluate the production of ROS. A large amount of ROS was detected for the light-illuminated g-C_3N_4 system (Figure 3a), which was generated from the interaction of dissolved oxygen and conduction electrons in g-C_3N_4. However, the fluorescence was dramatically decreased in the presence of GSH, thus demonstrating that GSH could deplete the generated ROS to a large extent, as also shown by other research groups. When Cu^{2+}–g-C_3N_4 was irradiated with light, we found that more ROS could be generated than with g-C_3N_4, thus indicating that the ligation of Cu^{2+} could increase the amount of ROS. Surprisingly, in the presence of GSH, the decrease in the fluorescence intensity of DCF with light-irradiated Cu^{2+}–g-C_3N_4 (26.30%) was lower than that with light-irradiated g-C_3N_4 (80.05%). This result suggested that ROS consumption by GSH was inhibited to a large extent by

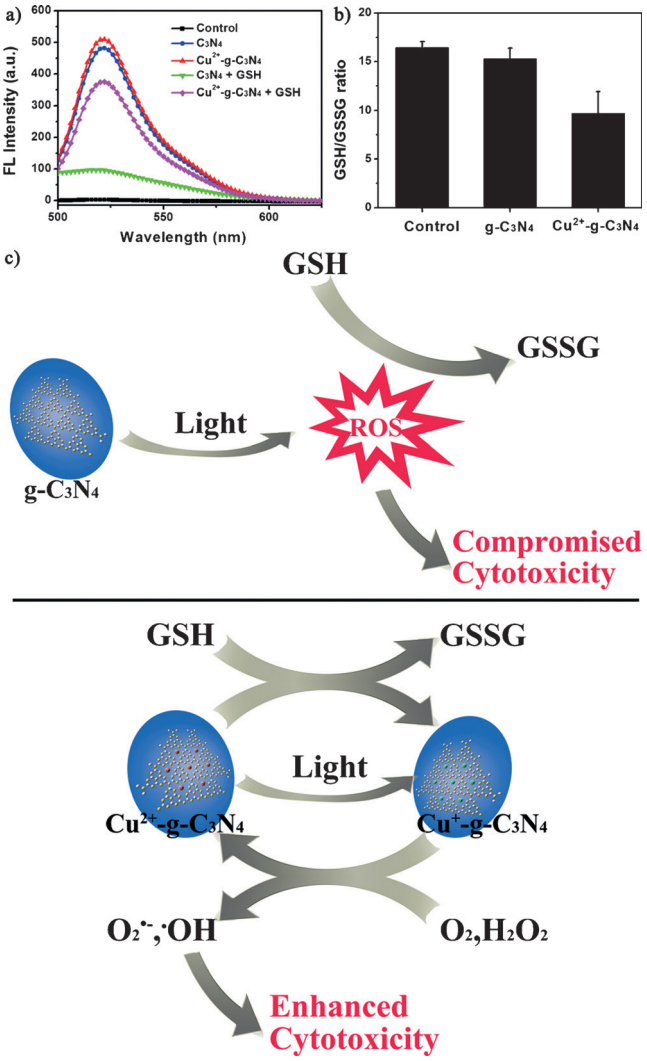

Figure 3. a) Fluorescence spectra of DCFH incubated with g-C_3N_4 or Cu^{2+}–g-C_3N_4 in the presence or absence of GSH (1 mM) under light irradiation. b) GSH/GSSH ratios of solutions containing GSH and g-C_3N_4 or Cu^{2+}–g-C_3N_4 under light irradiation, as examined with a commercial kit. c) Proposed mechanism of the reaction.

the ligation of Cu^{2+}. Additionally, ROS generation by Cu^{2+}–g-C_3N_4 was enhanced as the concentration of Cu^{2+}–g-C_3N_4 increased and as the concentration of GSH decreased (see Figures S6 and S7). The fluorescence probes hydroethidium and terephthalate were used to confirm that the generation of the superoxide radical and hydroxyl radical by Cu^{2+}–g-C_3N_4 was improved (see Figures S8 and S9).

Next, to verify the effect of Cu^{2+}–g-C_3N_4 on ROS depletion by GSH, we determined the ratio of reduced (GSH) to oxidized (GSSH) glutathione, an indication of oxidative stress levels. It was reported that Cu^{2+} could react with GSH through a metal-reducing action.[11] Accordingly, Cu^{2+}–g-C_3N_4 caused a decrease in the cellular GSH/GSSH ratio as compared with that of the control or g-C_3N_4 group (Figure 3b; see also Figure S10). Noting that the concentration of oxidative GSH (30 μM) in the presence of Cu^{2+}–g-C_3N_4 was three orders of magnitude higher than the concentration

of Cu^{2+} (0.03 μM) in the Cu^{2+}–g-C_3N_4, we propose a recycling mechanism for this phenomenon. As shown in Figure 3c, the presence of GSH could compromise the effect of ROS generated by g-C_3N_4. In constrast, Cu^{2+}–g-C_3N_4 could interact with GSH or be irradiated to generate redox-active species, Cu^{+}–g-C_3N_4, which could be oxidized to Cu^{2+}–g-C_3N_4 in the presence of molecular oxygen and hydrogen peroxide. This recycling ensured that the reduced GSH level was not restricted by the content of Cu in the system. Besides the smaller influence of GSH on the ROS, the additional generated hydroxyl radical could also contribute to the enhanced PDT efficiency. Taken together, all the above results manifested the capability of Cu^{2+}–g-C_3N_4 for enhanced ROS generation under light irradiation through the synergy of a Cu^{2+}-induced pro-oxidant effect and GSH oxidation.

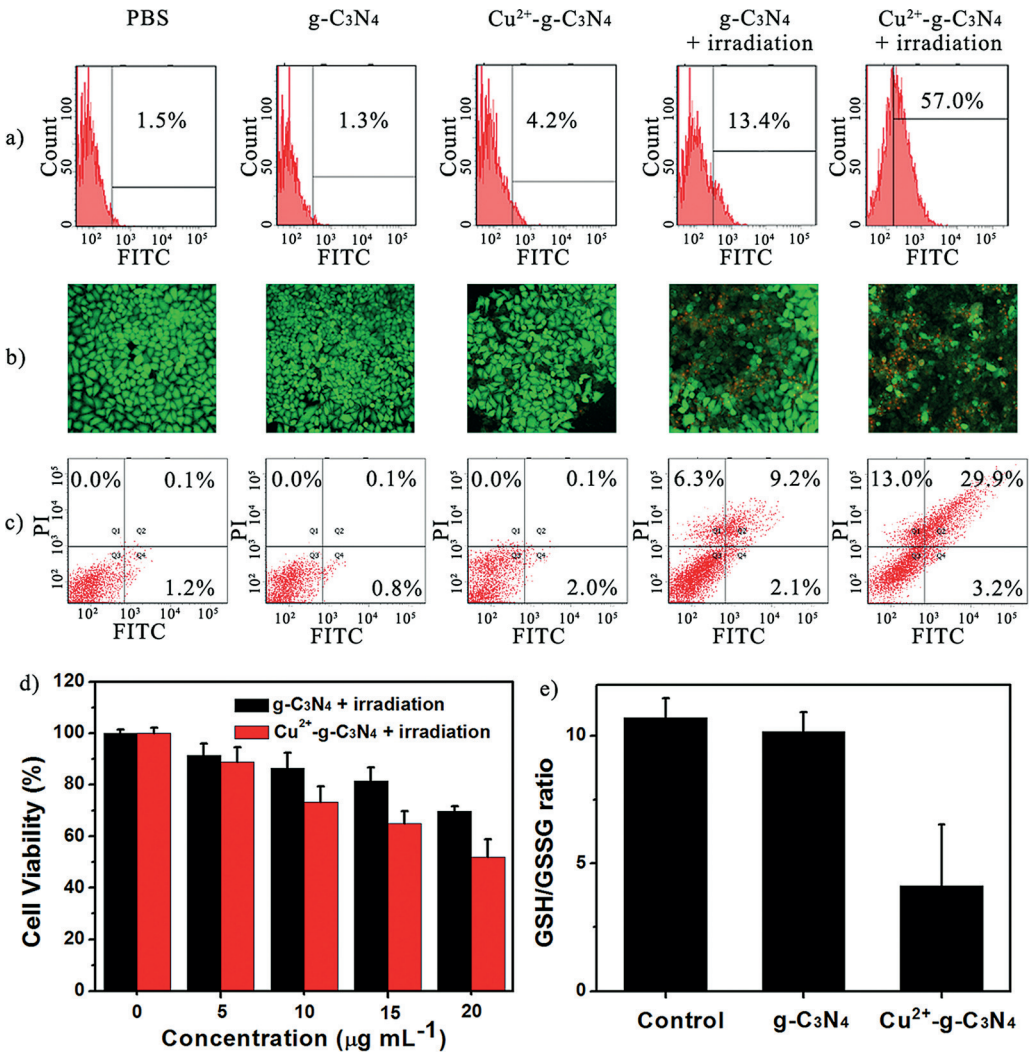

Figure 4. a) Flow cytometry analysis of ROS generation in cancer cells treated with different agents with or without light irradiation, as detected with 6-carboxy-2′,7′-dichlorodihydrofluorescein diacetate. b) Fluorescence images of Calcein AM- and PI-costained cells with different treatments. c) Flow cytometry analysis of apoptosis cells following treatment with different formulations. d) Cytotoxicity of g-C_3N_4 and Cu^{2+}–g-C_3N_4 at different concentrations under irradiation. e) Intracellular GSH/GSSH ratios of cells treated with g-C_3N_4 and Cu^{2+}–g-C_3N_4.

Encouraged by the observed enhanced production of ROS, we next investigated the PDT efficiency of Cu^{2+}–g-C_3N_4 in cancer cells. Differently treated HeLa cells were stained with dichlorofluorescein diacetate (DCFH-DA), and then the levels of intracellular ROS were measured by flow cytometry. A negligible percentage of cells treated with g-C_3N_4 or PBS showed green fluorescence (<2.0%), whereas cells treated with Cu^{2+}–g-C_3N_4 showed a slight increase in this percentage (4.2%; Figure 4a). After irradiation, the percentage of cells treated with g-C_3N_4 or Cu^{2+}–g-C_3N_4 that showed green fluorescence greatly increased, thus indicating that a large amount of ROS were generated. Notably, the percentage (57.0%) in cells treated with Cu^{2+}–g-C_3N_4 under light irradiation was much higher than that of g-C_3N_4 (13.4%) under the same conditions, thus suggesting the improved performance of Cu^{2+}–g-C_3N_4 as the ROS producer in cancer cells. To identify the phototoxicity of the Cu^{2+}–g-C_3N_4 system, we conducted a Calcein AM/prodium iodide cell-survival assay to differentiate live (green fluorescence) and dead cells (red fluorescence). We found no significant cytotoxicity in cells treated with PBS, g-C_3N_4, or Cu^{2+}–g-C_3N_4 (Figure 4b). After irradiation with light, a significant amount of dead cells were observed in cells treated with g-C_3N_4 and Cu^{2+}–g-C_3N_4. This result was attributed to the cytotoxicity of the ROS generated under these conditions. Fluorescein–annexin V and propidium iodide (PI) staining assays also demonstrated that the cell toxicity was associated with apoptosis or necrosis (Figure 4c). Moreover, quantitative analysis showed that the irradiation of Cu^{2+}–g-C_3N_4 with light led to more dead cells than that of g-C_3N_4, which was consistent with the amount of intracellularly generated ROS. This result was further confirmed by the MTT cell-viability assay (MTT = 3-(4,5-dimethylthiazol-2-yl)-2,5-diphenyltetrazolium bromide; Figure 4d; see also Figure S11). The intracellular GSH/GSSH ratio was found to decrease in cells treated with Cu^{2+}–g-C_3N_4, which suggested

that GSH oxidation was beneficial to the efficiency of PDT (Figure 4 f). These results suggested that Cu^{2+}–g-C_3N_4 could greatly improve ROS generation and PDT efficiency in cancer cells.

In conclusion, we have demonstrated the integration of Cu^{2+} and g-C_3N_4 with enhanced efficacy for photodynamic therapy in cancer cells. Cu^{2+}–g-C_3N_4 could interact with GSH through a metal-reducing action to reduce the intracellular GSH levels. Moreover, additional generated hydroxyl radicals could also contribute to the enhanced PDT efficiency. Thus, the enhancement was due to a combination of the Cu^{2+}-induced additional generation of ROS and reduced GSH levels. This coupled metal–inorganic hybrid system provides a new way to reduce intracellular GSH levels and improve the efficiency of photodynamic therapy. Additionally, it can be readily extended to improve performance in other applications, such as the degradation of organic materials, hydrogen evolution, and solar cells.

Acknowledgments

We acknowledge financial support by the 973 Project (2011CB936004) and the NSFC (21210002, 21431007, 21533008).

Keywords: glutathione · graphitic carbon nitride · photodynamic therapy · reactive oxygen species · synergetic effects

How to cite: *Angew. Chem. Int. Ed.* **2016**, *55*, 11467–11471
Angew. Chem. **2016**, *128*, 11639–11643

[1] a) C. Backes, N. C. Berner, X. Chen, P. Lafargue, P. LaPlace, M. Freeley, G. S. Duesberg, J. N. Coleman, A. R. McDonald, *Angew. Chem. Int. Ed.* **2015**, *54*, 2638–2642; *Angew. Chem.* **2015**, *127*, 2676–2680; b) X. Huang, C. L. Tan, Z. Y. Yin, H. Zhang, *Adv. Mater.* **2014**, *26*, 2185–2204; c) M. Chhowalla, Z. Liu, H. Zhang, *Chem. Soc. Rev.* **2015**, *44*, 2584–2586; d) H. Zhang, *ACS Nano* **2015**, *9*, 9451–9469.

[2] C. L. Tan, Z. D. Liu, W. Huang, H. Zhang, *Chem. Soc. Rev.* **2015**, *44*, 2615–2628.

[3] D. Deng, K. S. Novoselov, Q. Fu, N. Zheng, Z. Tian, X. Bao, *Nat. Nanotechnol.* **2016**, *11*, 218–230.

[4] a) X. Peng, L. L. Peng, C. Z. Wu, Y. Xie, *Chem. Soc. Rev.* **2014**, *43*, 3303–3323; b) Y. F. Sun, S. Gao, Y. Xie, *Chem. Soc. Rev.* **2014**, *43*, 530–546.

[5] D. Chimene, D. L. Alge, A. K. Gaharwar, *Adv. Mater.* **2015**, *27*, 7261–7284.

[6] a) X. D. Zhang, X. Xie, H. Wang, J. J. Zhang, B. C. Pan, Y. Xie, *J. Am. Chem. Soc.* **2013**, *135*, 18–21; b) X. Zhang, H. Wang, H. Wang, Q. Zhang, J. Xie, Y. Tian, J. Wang, Y. Xie, *Adv. Mater.* **2014**, *26*, 4438–4443; c) F. Goettmann, A. Thomas, M. Antonietti, *Angew. Chem. Int. Ed.* **2007**, *46*, 2717–2720; *Angew. Chem.* **2007**, *119*, 2773–2776; d) X. C. Wang, K. Maeda, A. Thomas, K. Takanabe, G. Xin, J. M. Carlsson, K. Domen, M. Antonietti, *Nat. Mater.* **2009**, *8*, 76–80; e) Y. Zheng, Y. Jiao, J. Chen, J. Liu, J. Liang, A. Du, W. Zhang, Z. Zhu, S. C. Smith, M. Jaroniec, G. Q. Lu, S. Z. Qiao, *J. Am. Chem. Soc.* **2011**, *133*, 20116–20119; f) T. Y. Ma, S. Dai, M. Jaroniec, S. Z. Qiao, *Angew. Chem. Int. Ed.* **2014**, *53*, 7281–7285; *Angew. Chem.* **2014**, *126*, 7409–7413; g) M. Xiong, Q. Rong, H. M. Meng, X. B. Zhang, *Biosens. Bioelectron.* **2016**, DOI: 10.1016/j.bios.2016.03.043.

[7] a) L.-S. Lin, Z.-X. Cong, J. Li, K.-M. Ke, S.-S. Guo, H.-H. Yang, G.-N. Chen, *J. Mater. Chem. B* **2014**, *2*, 1031; b) R. Chen, J. Zhang, Y. Wang, X. Chen, J. A. Zapien, C. S. Lee, *Nanoscale* **2015**, *7*, 17299–17305; c) H. Wan, Y. Zhang, W. Zhang, H. Zou, *ACS Appl. Mater. Interfaces* **2015**, *7*, 9608–9618.

[8] a) F. Jiang, A. M. Robin, M. Katakowski, L. Tong, M. Espiritu, G. Singh, M. Chopp, *Laser Med. Sci.* **2003**, *18*, 128–133; b) M. D. Hall, T. W. Hambley, *Coord. Chem. Rev.* **2002**, *232*, 49–67.

[9] H. Fan, G. Yan, Z. Zhao, X. Hu, W. Zhang, H. Liu, X. Fu, T. Fu, X. B. Zhang, W. Tan, *Angew. Chem. Int. Ed.* **2016**, *55*, 5477–5482; *Angew. Chem.* **2016**, *128*, 5567–5572.

[10] a) C. Santini, M. Pellei, V. Gandin, M. Porchia, F. Tisato, C. Marzano, *Chem. Rev.* **2014**, *114*, 815–862; b) J. Wang, C. Luo, C. Shan, Q. You, J. Lu, S. Elf, Y. Zhou, Y. Wen, J. L. Vinkenborg, J. Fan, H. Kang, R. Lin, D. Han, Y. Xie, J. Karpus, S. Chen, S. Ouyang, C. Luan, N. Zhang, H. Ding, M. Merkx, H. Liu, J. Chen, H. Jiang, C. He, *Nat. Chem.* **2015**, *7*, 968–979.

[11] H. Speisky, M. Gómez, C. Carrasco-Pozo, E. Pastene, C. Lopez-Alarcón, C. Olea-Azar, *Bioorg. Med. Chem.* **2008**, *16*, 6568–6574.

[12] M. F. Poyton, A. M. Sendecki, X. Cong, P. S. Cremer, *J. Am. Chem. Soc.* **2016**, *138*, 1584–1590.

[13] a) Y. Zhang, K. Aslan, M. J. Previte, C. D. Geddes, *J. Fluoresc.* **2007**, *17*, 345–349; b) S. Y. Lee, T. Yasuda, Y. S. Yang, Q. Zhang, C. Adachi, *Angew. Chem. Int. Ed.* **2014**, *53*, 6402–6406; *Angew. Chem.* **2014**, *126*, 6520–6524.

[14] Y. Y. Yuan, C. J. Zhang, R. T. K. Kwok, S. D. Xu, R. Y. Zhang, J. Wu, B. Z. Tang, B. Liu, *Adv. Funct. Mater.* **2015**, *25*, 6586–6595.

[15] Y. Li, Z. Wang, T. Xia, H. Ju, K. Zhang, R. Long, Q. Xu, C. Wang, L. Song, J. Zhu, J. Jiang, Y. Xiong, *Adv. Mater.* **2016**, DOI: 10.1002/adma.201601960.

[16] a) J. Ghijsen, L. H. Tjeng, J. van Elp, H. Eskes, J. Westerink, G. A. Sawatzky, M. T. Czyzyk, *Phys. Rev. B* **1988**, *38*, 11322–11330; b) Y. D. Zhu, J. Peng, L. P. Jiang, J. J. Zhu, *Analyst* **2014**, *139*, 649–655.

Received: June 6, 2016
Published online: August 9, 2016

